Int. J. Multiphase Flow Vol. 10, No. 4, pp. 401–413, 1984
Printed in the U.S.A.

0301-9322/84 $3.00 + .00
Pergamon/Elsevier

CRITICAL HEAT FLUX OF LIQUID HELIUM (I) IN FORCED CONVECTIVE BOILING

Y. KATTO and S. YOKOYA
Department of Mechanical Engineering, University of Tokyo, Hongo, Bunkyo-ku, Tokyo, Japan

(*Received* 21 *June* 1983; *in revised form* 15 *December* 1983)

Abstract—For liquid helium (I) flowing through a uniformly heated vertical tube of 1 mm i.d., critical heat flux (CHF) of forced convective boiling has been measured under the conditions of a pressure of 0.199 MPa with vapor-to-liquid density ratio of 0.409, length-to-diameter ratios from 25 to 200, mass velocities from 11 to 108 kg m^{-2} s^{-1}, and inlet subcooling enthalpy from −3.5 to +7.0 kJ kg^{-1}. The experimental results thus obtained are analyzed revealing that the high pressure character, which has already been observed for water and Freons at extremely high pressures, is certainly found at high mass velocities for liquid helium too, though its appearance is restricted within very narrow limits due to the phenomenon that the wall temperature situation identifying the CHF condition fades away when the mass velocity becomes high.

1. INTRODUCTION

This paper deals with the critical heat flux (CHF) of forced convective boiling in uniformly heated vertical tubes with subcooled inlet conditions. In this case, it has been known for water and Freons that the CHF at high mass velocities exhibits a quite different character at extremely high pressures (say, $\rho_G/\rho_L > 0.15$) from that at ordinary pressures (say, $\rho_G/\rho_L < 0.15$). Curiously enough, however, the "high pressure character" mentioned above is not found for the existing data of liquid helium, and the chronological situations of this problem are as follows.

1.1 *High pressure character looked at from the existing data of water and liquid helium*

As for the existing data of the CHF of water at extremely high pressures, a number of data were collected in tables 11–14 of the paper of Thompson & Macbeth (1964), and others were presented by Peskov *et al.* (1969), Becker *et al.* (1972), Campolunghi *et al.* (1974), Chojnowski *et al.* (1974), Watson & Lee (1974), Doroschuk *et al.* (1975) and others. Empirical correlation equations applicable to the high pressure data such as mentioned above were then proposed by Peskov *et al.* (1969), Lee (1970) and Becker *et al.* (1972), disclosing the existence of the high pressure character for water. The lower limit of the mass velocity to exhibit the high pressure character for water was also given as a function of pressure in the foregoing paper of Becker *et al.*

Meanwhile, the condition of high density ratio $\rho_G/\rho_L > 0.15$ is frequently encountered with liquid helium employed for cooling purposes, because this condition is fulfilled by saturated helium at pressures higher than 1.09 atm. The CHF of liquid helium was measured under such condition by Ogata & Sato (1973), Giarratano *et al.* (1974), Keilin *et al.* (1975) and others employing tubes of very small diameters from 1.0 to 2.2 mm. A few empirical correlations of those data were proposed; but since there were no experiments made for much lower magnitudes of ρ_G/ρ_L, no investigators referred to the high pressure character of CHF for liquid helium.

Incidentally, Katto (1980a, b) attempted to correlate the existing CHF data of various fluids for forced convective boiling in uniformly heated vertical tubes. In this correlation, the critical heat flux q_c for the inlet subcooling enthalpy ΔH_i and the latent heat of evaporation H_{LG} was written as:

$$q_c = q_{c0}(1 + K \cdot \Delta H_i/H_{LG}) \qquad [1]$$

and the basic quantities q_{c0} and K on the r.h.s. of [1] were correlated in generalized forms, respectively. As the result, the most important q_{c0} among the two was predicted by the lowest among the three values of q_{c0} given by the following equations [2]–[4]:

$$\frac{q_{c0}}{GH_{LG}} = C\left(\frac{\sigma\rho_L}{G^2 l}\right)^{0.043} \frac{1}{l/d} \qquad [2]$$

$$\frac{q_{c0}}{GH_{LG}} = 0.10\left(\frac{\rho_G}{\rho_L}\right)^{0.133}\left(\frac{\sigma\rho_L}{G^2 l}\right)^{1/3} \frac{1}{1+0.0031\, l/d} \qquad [3]$$

$$\frac{q_{c0}}{GH_{LG}} = 0.098\left(\frac{\rho_G}{\rho_L}\right)^{0.133}\left(\frac{\sigma\rho_L}{G^2 l}\right)^{0.433} \frac{(l/d)^{0.27}}{1+0.0031\, l/d} \qquad [4]$$

where G is the mean mass velocity through the tube, σ the surface tension, ρ_L the density of liquid, l the heated length of tube, d the internal diameter of tube, ρ_G the density of vapor. The value of a parameter C on the r.h.s. of [2] is 0.25 for $l/d < 50$, $0.25 + 0.0009\{(l/d) - 50\}$ for $l/d = 50 - 150$, and 0.34 for $l/d > 150$.

When the mass velocity G is increased from a low value under the condition of fixing all other factors, q_{c0} is determined initially by [2], then by [3], and finally by [4] for sufficiently high values of G. [4] is distinguished from [2] and [3] by the nature that q_{c0} is nearly saturated as for the effect of $G(q_{c0} \propto G^{0.134})$. Roughly speaking, q_{c0} predicted by [2] and [3] corresponds to the liquid film dryout-type CHF, while that of [4] to the DNB-type CHF (see Katto 1982 for more details). The accuracy of the foregoing prediction may not be so high as applicable to the design purposes, but [2]–[4] can predict q_{c0} fairly well for various fluids as shown in the paper of Katto (1980a).

However, the CHF data of water at extremely high pressures disagree with the prediction of [4], because they exhibit the high pressure character suggested by the empirical correlations of Peskov *et al.* (1969), Lee (1970), and Becker *et al.* (1972) that q_{c0} increases greatly with increasing G. Hence, the following equation [5] was added to the Katto correlation so as to fit in with the above-mentioned water data.

$$\frac{q_{c0}}{GH_{LG}} = 0.0384\left(\frac{\rho_G}{\rho_L}\right)^{0.60}\left(\frac{\sigma\rho_l}{G^2 l}\right)^{0.173} \frac{1}{1+0.280\left(\frac{\sigma\rho_L}{G^2 l}\right)^{0.233}\frac{l}{d}} \qquad [5]$$

However, the existing data of liquid helium mentioned before were found to agree with [4] instead of [5] in spite of having very high values of ρ_G/ρ_L (see figure 9 of Katto & Ashida 1982); and it was noticed that the systematic experimental data of water employed to derive [5] were in the range of $l/d > 110$, while the data of liquid helium were in the range of $l/d \leqq 51$. Then, taking into account the foregoing experimental facts, Katto (1980b) tentatively derived a sophisticated criterion to specify the applicable range of [5].

1.2 *Facts revealed by the experiments of Freons*

The foregoing equation [5] as well as the criterion of specifying the applicable range of [5] was based on the data of only water and liquid helium. Therefore, Katto & Yokoya (1982) attempted an experimental study of CHF by employing R-12 in the ranges of $\rho_G/\rho_L = 0.109$–0.306, $l/d = 200$–333, and $G = 1100$–$8800\ \mathrm{kg\,m^{-2}\,s^{-1}}$, with the purpose to test the general applicability of [5]. The R-12 data thus obtained under the condition of $l/d = 200$–333 showed a good agreement with the prediction of [5] for $\rho_G/\rho_L \geqq 0.18$. Katto and Ashida (1982) then extended the experiment of R-12 to the case of $l/d = 50$ in order to test [5] in the region where [5] was postulated to be unapplicable. Contrary to

expectation, however, it disclosed that the data of R-12 for $l/d = 50$ and $\rho_G/\rho_L \geqq 0.18$ agreed with the prediction of [5].

In addition to these studies, Nishikawa *et al.* (1982) investigated the CHF of R-22 and R-115 under the condition of $\rho_G/\rho_L > 0.18$, covering the ranges of $\rho_G/\rho_L = 0.187$–0.517 and $G = 200$–$1300\,\mathrm{kg\,m^{-2}\,s^{-1}}$ for R-22, and the ranges of $\rho_G/\rho_L = 0.187$–0.394 and $G = 400$–$1300\,\mathrm{kg\,m^{-2}\,s^{-1}}$ for R-115. Though the experiments were done with a single tube of $l/d = 154$, Nishikawa *et al.* estimated q_{c0} for various values of l/d employing the boiling length concept. The data of q_{c0} thus obtained at high G agree fairly well with the trend of [5] for $l/d > 10$.

1.3 *Aim of the present study*

The results mentioned so far indicate that various fluids exhibit the high pressure character at very high ρ_G/ρ_L independent of the magnitude of l/d, including water, R-12, R-22 and R-115. However, the existing data of liquid helium are restricted to the range of $l/d \leqq 51$, and besides have a singular behavior not exhibiting the high pressure character in spite of high values of ρ_G/ρ_L.

The present study is initiated with the aim to study the following two problems: (i) whether or not liquid helium is a special material not exhibiting the high pressure character for $l/d \leqq 51$, and (ii) what kind of character is observed for the CHF of liquid helium in the range of $l/d > 51$. The occurrence of the high pressure character will be examined below by comparing the q_{c0} data with [4] and [5], because these generalized equations are applicable to water and Freons at least as has been mentioned before.

2. EXPERIMENTAL APPARATUS

2.1 *Experimental apparatus*

The experimental apparatus employed in this study is illustrated schematically in figure 1. The helium gas of 99.99% purity fed from the gas bombs shown on the lower right-hand corner of figure 1 goes through the pressure regulator and the flow meters, and thereafter flows along a thick directed line. This flowing helium gas is precooled in the liquid nitrogen cryostat, and then cooled in the liquid helium cryostat so as to be liquefied before entering the test chamber, where the CHF is measured. The two-phase flow of helium coming out of the test chamber goes through the regenerative heat exchangers equipped in the LHe and LN_2 cryostats respectively to cool the incoming helium gas, and finally is released to the surrounding atmosphere through the pressure control valves. In the foregoing two cryostats, the saturated liquid nitrogen and liquid helium are stored at atmospheric pressure to cool and liquefy the passing helium gas, both being insulated from the surrounding by means of the vacuum walls evacuated up to about 10^{-3}–10^{-4} Pa.

2.2 *Test chamber*

The test chamber, which is submerged in the pool of stored liquid helium as shown in figure 1, is a cylindrical vessel of 50 mm dia. and 450 mm length being evacuated up to about 10^{-3}–10^{-4} Pa for the purpose of insulation. The inside of the test chamber is illustrated in figure 2, where the subcooled liquid helium entering from the bottom is regulated in temperature by the preheater before flowing into the test tube of stainless steel, with which the CHF is measured.

The preheater is heated by an insulated Manganin wire wound around the preheater tube, while the test tube of 1.0 mm i.d. and 1.5 mm o.d. is heated by direct passage of an electric current. The power input wires, which supply d.c. current to the abovementioned preheater and test tube, are immersed directly in the liquid helium outside of the test chamber in order to prevent the flow of heat from the surroundings to the test chamber.

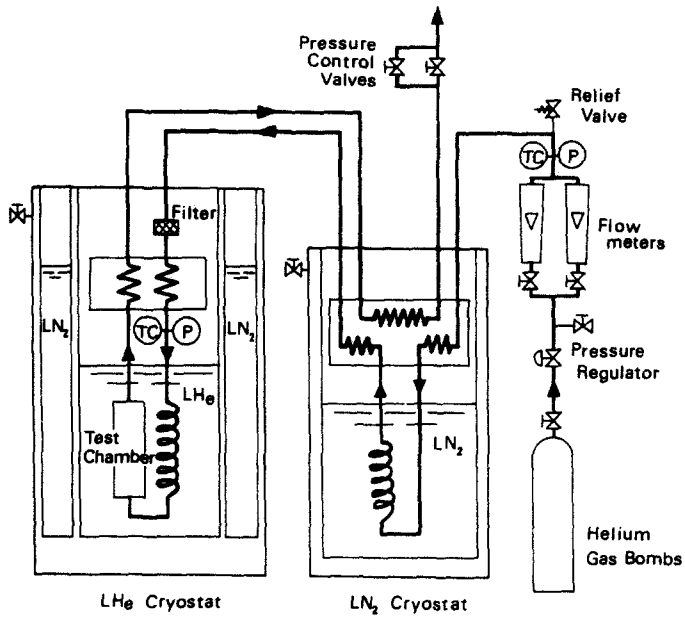

Figure 1. Experimental apparatus (TC: thermocouple, P: pressure gauge).

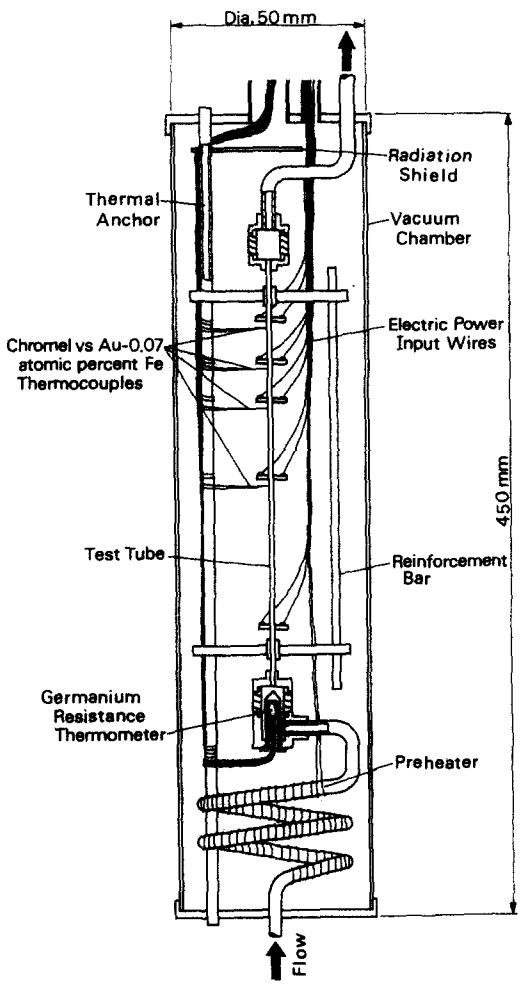

Figure 2. Test chamber.

In addition, as is seen in figure 2, these wires are so arranged as to change the heated length of the test tube by means of the outside switching. The heat flux from the test tube is measured with the accuracy of $\pm 2.5\,\mathrm{W\,m^{-2}}$.

The temperature of the fluid entering the test tube is measured by the germanium resistance thermometer equipped in a mixing chamber at the tube inlet with the accuracy of ± 0.01 K. Simultaneous measurements of wall temperatures are made by four thermocouples of chromel vs Au-0.07 atomic per cent Fe, each being located at the position 5 mm upstream of the exit end of the heated section set up in the way mentioned before.

Leading wires for the abovementioned thermometer and thermocouples are wound respectively around the thermal anchor as shown in figure 2. This thermal anchor is a metal tube capable of passing the surrounding liquid helium through it, and thereby the heat invading through the leading wires can be absorbed. The radiation shield mounted near the top end of the test chamber is a 1 mm thick metal plate, which prevents the thermal radiation coming downward through the hole passing the leading wires.

2.3 *System pressure, mass velocity and inlet subcooling enthalpy*

The system pressure p is measured by the pressure gauge located upstream of the test chamber as is seen in figure 1 with the accuracy of ± 2 KPa. The mass velocity G can be evaluated by the flow meters with the accuracy of ± 0.6 kg m^{-2} s^{-1}. Inlet subcooling enthalpy ΔH_i is determined by the following principle. In the present experiment, helium is fed to the system from the gas bombs with sufficiently high pressures. Thus, once a prescribed flow state of liquid helium is established at the inlet to the test chamber, it remains unchanged when the preheater and the test tube are heated. This means that the enthalpy of liquid helium H_p at the inlet of the preheater is kept constant independent of the electric power input E_p to the preheater, and H_p is readily measured by the germanium resistance thermometer under the condition of $E_p = 0$. With the value of H_p thus determined, the inlet subcooling enthalpy ΔH_i at the inlet of the test tube is readily known as follows:

$$\Delta H_i = H_s - (H_p + E_p/W) \qquad [6]$$

where H_s is the enthalpy of the saturated liquid helium at the system pressure and W the feeding rate of helium to the test tube. If the power input E_p is raised enough, experiments can be extended in some measure to the two-phase mixed inlet condition ($\Delta H_i < 0$). The error in measuring ΔH_i is presumed to be within $\pm 2\%$.

3. EXPERIMENTAL RESULTS

3.1 *Experimental ranges*

In this study, experiments of helium (I) have been made covering the following ranges:

$p = 0.199$ MPa (corresponding saturation temperature $T_s = 5.02$ K, latent heat of evaporation $H_{LG} = 11.3\,\mathrm{kJ\,kg^{-1}}$, and density ratio $\rho_G/\rho_L = 0.409$), $d = 1$ mm, $l/d = 25$, 50, 100 and 200 and $\Delta H_i = -3.5$ to $+7.5\,\mathrm{kJ\,kg^{-1}}$.

The test tube diameter of 1 mm is very small as compared with those employed usually in the CHF experiments of ordinary fluids, but it may possibly be regarded as an unserious problem because the vapor-to-liquid density ratio ρ_G/ρ_L is extremely high and the surface tension σ is extremely low ($\sigma = 1.81 \times 10^{-5}\,\mathrm{N\,m^{-1}}$) for helium at the test pressure of 0.199 MPa.

3.2 *Experimental results*

All the experimental data of CHF obtained in the present study are listed in table 1 and are represented in figures 3 and 4. Referring to those data, the following two observations must be reported.

Table 1. Critical heat flux data for liquid helium together with exit quality X_{ex}, basic CHF q_{c0} and inlet subcooling K

EXPT NO	p	d	l/d	G	ΔH_i	q_c	X_{ex}	q_{co}	K
	MPa	mm		kg/m^{2}s	kJ/kg	kW/m^2		kW/m^2	
1	0.199	1.0	25	10.47	5.3740	1.1610	0.50570	0.7748	1.0740
2	0.199	1.0	25	10.47	3.5280	1.0230	0.55240		
3	0.199	1.0	25	10.47	1.7770	0.9279	0.62700		
4	0.199	1.0	25	10.47	-0.0683	0.7982	0.68070		
5	0.199	1.0	25	10.47	-1.8920	0.6062	0.67980		
6	0.199	1.0	25	17.46	5.3740	1.2600	0.16300	0.8418	1.0940
7	0.199	1.0	25	17.46	3.5400	1.1630	0.27610		
8	0.199	1.0	25	17.46	1.7170	0.9688	0.33900		
9	0.199	1.0	25	17.46	-0.1061	0.8399	0.43500		
10	0.199	1.0	25	17.46	-1.9190	0.6785	0.51370		
11	0.199	1.0	25	24.48	5.5360	1.4260	0.02558	0.9642	0.9962
12	0.199	1.0	25	24.48	2.9220	1.2140	0.18020		
13	0.199	1.0	25	24.48	0.3317	1.0160	0.33790		
14	0.199	1.0	25	24.48	-2.2490	0.7568	0.47260		
15	0.199	1.0	25	35.02	5.5360	1.6620	-0.06992	1.0910	1.0970
16	0.199	1.0	25	35.02	3.7170	1.4820	0.04556		
17	0.199	1.0	25	35.02	1.8880	1.3180	0.16590		
18	0.199	1.0	25	35.02	0.0780	1.1130	0.27430		
19	0.199	1.0	25	35.02	-1.7390	0.8835	0.37710		
20	0.199	1.0	25	52.97	5.5900	2.0340	-0.15480	1.2740	1.2290
21	0.199	1.0	25	52.97	4.3880	1.9030	-0.07038		
22	0.199	1.0	25	52.97	3.1520	1.7140	0.00742		
23	0.199	1.0	25	52.97	1.9600	1.5380	0.08349		
24	0.199	1.0	25	52.97	0.7238	1.3690	0.16460		
25	0.199	1.0	25	52.97	-0.4781	1.2130	0.24490		
26	0.199	1.0	25	52.97	-1.5040	1.0640	0.31080		
27	0.199	1.0	25	70.84	5.5360	2.5960	-0.16560	1.6840	1.1220
28	0.199	1.0	25	70.84	4.6750	2.4480	-0.10790		
29	0.199	1.0	25	70.84	3.5740	2.3060	-0.02821		
30	0.199	1.0	25	70.84	2.0930	2.0980	0.07686		
31	0.199	1.0	25	70.84	1.1890	1.8400	0.12460		
32	0.199	1.0	25	70.84	0.3076	1.7130	0.18670		
33	0.199	1.0	25	70.84	-0.6051	1.5950	0.25280		
34	0.199	1.0	25	70.84	-1.5530	1.4210	0.31490		
35	0.199	1.0	25	82.01	6.0000	3.1550	-0.19050	2.1510	0.8973
36	0.199	1.0	25	82.01	4.4400	2.9150	-0.07836		
37	0.199	1.0	25	82.01	2.8770	2.6770	0.03426		
38	0.199	1.0	25	82.01	1.3360	2.3790	0.13840		
39	0.199	1.0	25	82.01	-0.2109	2.0970	0.24490		
40	0.199	1.0	25	89.51	5.3740	3.3210	-0.14720	------	------
41	0.199	1.0	25	89.51	4.6600	3.2430	-0.09176		
42	0.199	1.0	25	89.51	3.9490	3.3230	-0.02093		
43	0.199	1.0	25	89.51	3.2440	3.4980	0.05875		
44	0.199	1.0	25	89.51	1.1120	3.3300	0.23080		
45	0.199	1.0	25	89.51	-0.5049	3.0720	0.34830		
46	0.199	1.0	50	10.52	2.3900	0.6545	0.88960	0.5348	1.1040
47	0.199	1.0	50	10.52	-0.6638	0.5133	0.92230		
48	0.199	1.0	50	10.52	-2.6390	0.3888	0.88760		
49	0.199	1.0	50	17.58	5.0300	0.9419	0.50310	0.6460	1.0330
50	0.199	1.0	50	17.58	1.3800	0.7307	0.61350		
51	0.199	1.0	50	17.58	-0.4120	0.6192	0.65980		
52	0.199	1.0	50	17.58	-2.2590	0.5128	0.71610		
53	0.199	1.0	50	24.49	5.8480	1.1310	0.29980	0.7310	1.0510
54	0.199	1.0	50	24.49	3.1960	0.9436	0.39910		
55	0.199	1.0	50	24.49	0.5800	0.7718	0.50640		
56	0.199	1.0	50	24.49	-1.6900	0.6167	0.59520		
57	0.199	1.0	50	35.25	5.8480	1.2320	0.10100	0.7838	1.0850
58	0.199	1.0	50	35.25	4.0220	1.0800	0.18630		

Table 1 (*Contd.*)

EXPT NO	p	d	l/d	G	ΔH_i	q_c	X_{ex}	q_{co}	K
	MPa	mm		kg/m^2s	kJ/kg	kW/m^2		kW/m^2	
59	0.199	1.0	50	35.25	2.2180	0.9425	0.27690		
60	0.199	1.0	50	35.25	0.3901	0.8120	0.37310		
61	0.199	1.0	50	35.25	-1.3670	0.6915	0.46810		
62	0.199	1.0	50	35.25	-3.1140	0.5462	0.54980		
63	0.199	1.0	50	53.11	5.4280	1.6780	0.07884	1.0410	1.3060
64	0.199	1.0	50	53.11	4.2050	1.5610	0.14800		
65	0.199	1.0	50	53.11	3.0160	1.3910	0.19660		
66	0.199	1.0	50	53.11	1.8080	1.2820	0.26720		
67	0.199	1.0	50	53.11	0.5855	1.1310	0.32500		
68	0.199	1.0	50	53.11	-0.5499	0.9478	0.36450		
69	0.199	1.0	50	71.10	5.4280	2.3410	0.10230	1.3990	1.4300
70	0.199	1.0	50	71.10	3.6090	2.0590	0.19310		
71	0.199	1.0	50	71.10	1.8130	1.7360	0.27170		
72	0.199	1.0	50	71.10	0.9488	1.5620	0.30480		
73	0.199	1.0	50	71.10	0.0226	1.3890	0.34370		
74	0.199	1.0	50	89.30	4.5600	2.6270	0.11710	1.4930	1.8380
75	0.199	1.0	50	89.30	3.1060	2.1930	0.15970		
76	0.199	1.0	50	89.30	1.6750	1.9270	0.23360		
77	0.199	1.0	50	107.60	5.8480	3.5220	0.06181	------	------
78	0.199	1.0	50	107.60	5.2470	3.4390	0.10130		
79	0.199	1.0	50	107.60	4.6580	3.3500	0.13880		
80	0.199	1.0	50	107.60	4.0620	3.2680	0.17800		
81	0.199	1.0	50	107.60	3.4690	3.1810	0.21620		
82	0.199	1.0	50	107.60	2.8670	3.1010	0.25630		
83	0.199	1.0	50	107.60	2.2960	3.1030	0.30720		
84	0.199	1.0	100	10.56	5.4280	0.4100	0.89400	0.2663	1.1110
85	0.199	1.0	100	10.56	2.4230	0.3258	0.87760		
86	0.199	1.0	100	10.56	-0.6465	0.2526	0.90390		
87	0.199	1.0	100	10.56	-3.6450	0.1700	0.89240		
88	0.199	1.0	100	17.64	6.9500	0.5347	0.45790	0.3079	1.1850
89	0.199	1.0	100	17.64	3.2940	0.4094	0.53000		
90	0.199	1.0	100	17.64	-0.3000	0.3007	0.62990		
91	0.199	1.0	100	24.75	6.2490	0.6399	0.36210	0.3906	1.1590
92	0.199	1.0	100	24.75	3.6410	0.5349	0.44280		
93	0.199	1.0	100	24.75	1.0630	0.4398	0.53490		
94	0.199	1.0	100	24.75	-1.5070	0.3264	0.60010		
95	0.199	1.0	100	35.44	5.8480	0.9225	0.40380	0.4978	1.6820
96	0.199	1.0	100	35.44	4.0300	0.7955	0.43790		
97	0.199	1.0	100	35.44	2.2310	0.6778	0.47950		
98	0.199	1.0	100	35.44	0.4195	0.5360	0.49820		
99	0.199	1.0	100	35.44	-1.4090	0.3810	0.50520		
100	0.199	1.0	100	53.51	5.8480	1.1550	0.24650	0.6727	1.3020
101	0.199	1.0	100	53.51	4.6540	1.0150	0.25950		
102	0.199	1.0	100	53.51	3.4580	0.9216	0.30360		
103	0.199	1.0	100	53.51	2.2350	0.8367	0.35570		
104	0.199	1.0	100	53.51	1.0410	0.7554	0.40750		
105	0.199	1.0	100	53.51	-0.1185	0.6786	0.45930		
106	0.199	1.0	100	71.21	4.5600	1.4690	0.32660	0.8433	1.7900
107	0.199	1.0	100	71.21	3.6550	1.3070	0.32620		
108	0.199	1.0	100	71.21	2.7600	1.2080	0.35620		
109	0.199	1.0	100	71.21	1.8600	1.1080	0.38610		
110	0.199	1.0	100	71.21	0.9487	0.9662	0.39630		
111	0.199	1.0	100	89.38	5.8480	2.0770	0.30500	------	------
112	0.199	1.0	100	89.38	5.1290	2.0170	0.34490		
113	0.199	1.0	100	89.38	4.0760	2.0110	0.43570		
114	0.199	1.0	100	89.38	3.7030	1.9450	0.44260		
115	0.199	1.0	100	89.38	2.9770	2.0780	0.55950		
116	0.199	1.0	100	89.38	2.2960	2.0120	0.59360		
117	0.199	1.0	100	89.38	1.5900	2.0140	0.65690		

Table 1 (*Contd.*)

EXPT NO	p	d	l/d	G	ΔH_i	q_c	X_{ex}	q_{co}	K
	MPa	mm		kg/m^{2}s	kJ/kg	kW/m^2		kW/m^2	
118	0.199	1.0	200	10.54	5.8480	0.1959	0.79830	0.1176	1.2790
119	0.199	1.0	200	10.54	2.7750	0.1574	0.81160		
120	0.199	1.0	200	10.54	-0.2713	0.1067	0.74070		
121	0.199	1.0	200	10.54	-3.2450	0.0783	0.81310		
122	0.199	1.0	200	17.59	5.8480	0.3131	0.74260	0.1779	1.5210
123	0.199	1.0	200	17.59	2.1850	0.2398	0.77170		
124	0.199	1.0	200	17.59	-1.4400	0.1386	0.68520		
125	0.199	1.0	200	24.59	5.4280	0.3963	0.66060	0.2259	1.6190
126	0.199	1.0	200	24.59	2.6080	0.3132	0.67090		
127	0.199	1.0	200	24.59	0.1416	0.2411	0.68160		
128	0.199	1.0	200	24.59	-2.3820	0.1405	0.61530		
129	0.199	1.0	200	35.31	5.8480	0.5226	0.53020	0.3183	1.2440
130	0.199	1.0	200	35.31	4.0180	0.4571	0.56090		
131	0.199	1.0	200	35.31	2.2100	0.3967	0.59980		
132	0.199	1.0	200	35.31	0.4088	0.3399	0.64530		
133	0.199	1.0	200	35.31	-1.4350	0.2627	0.65370		
134	0.199	1.0	200	52.64	6.2490	0.7875	0.50610	------	------
135	0.199	1.0	200	52.64	5.0280	0.7045	0.50250		
136	0.199	1.0	200	52.64	3.8120	0.6664	0.55890		
137	0.199	1.0	200	52.64	2.6100	0.7448	0.77070		
138	0.199	1.0	200	52.64	1.3670	0.7848	0.93450		

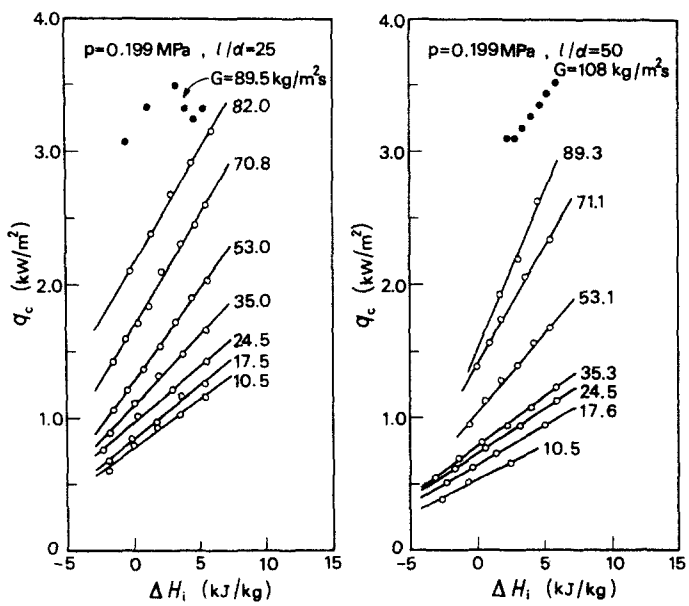

Figure 3. Experimental data of CHF of liquid helium ($l/d = 25$ and 50).

First, the rapid temperature excursion such as characterizing the CHF of ordinary fluids is not observed in the present experiment. Instead, it is found that there are two remarkable differences between the wall temperature situations before and after the occurrence of CHF: that is, after the onset of CHF, (i) the rate of wall temperature change on heat flux increase rises abruptly, and (ii) the wall temperature begins to fluctuate. The

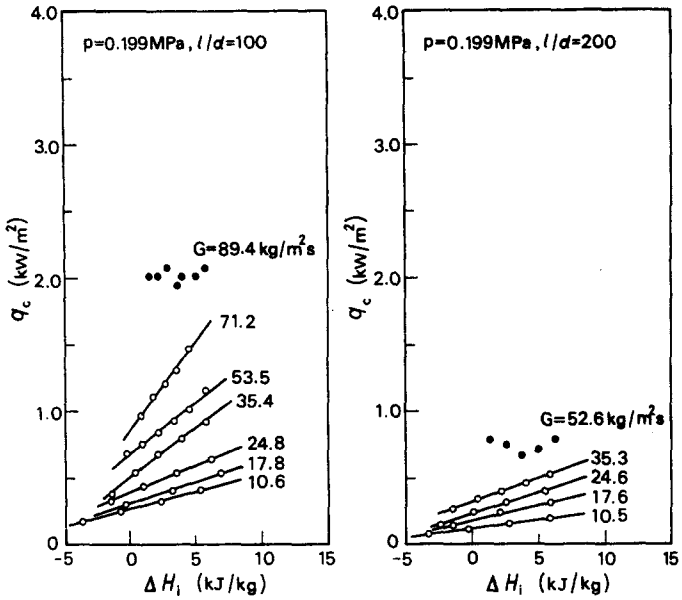

Figure 4. Experimental data of CHF of liquid helium ($l/d = 100$ and 200).

data points designated by open circles in figures 3 and 4 are those measured through the foregoing two discontinuous changes of the wall temperature situations.

Second, when the mass velocity G becomes comparatively high, the detection of CHF becomes impossible because the wall temperature begins to rise monotonously without any discontinuous change with increasing heat flux. The irregular data points represented by solid circles in figures 3 and 4 are those measured near the limit condition capable of detecting CHF by the two discontinuous changes of the wall temperature situations.

4. ANALYSIS OF DATA AND DISCUSSION

4.1 *Analysis of data*

It is noted for the regular CHF data in figures 3 and 4 that each family of data points for the same mass velocity G exhibits a linear relationship between the critical heat flux q_c and the inlet subcooling enthalpy ΔH_i within the experimental range of ΔH_i at least. Thus q_{c0} and K defined in [1] can be evaluated for each set of p, l/d and G. The experimental values of q_{c0} thus determined are compared with the predictions of [2]–[5] in figures 5 and 6. Roughly speaking, the experimental values agree fairly well with the predicted values though somewhat regular deviations are seen for $l/d = 100$ and 200.

4.2 *Appearance of high pressure character*

It can be seen in figure 5 that data points in the range of low $\sigma\rho_L/G^2l$ are certainly in accord with the prediction of [5] instead of [4]. Unfortunately those data points are quite limited in number (the reason will be described later in section 4.3), but it is of interest to note that there are no exceptional data as to the abovementioned trend of agreeing with the prediction of [5].

However, one thing must be examined in connection with the reliability of the data points, because the CHF in this study has been detected by the thermocouple located 5 mm upstream of the exit end of the heated section as has been described in section 2.2. If the virtual tube length $l^* = l - 5$ (mm) is used instead of the actual length l, and the effect of

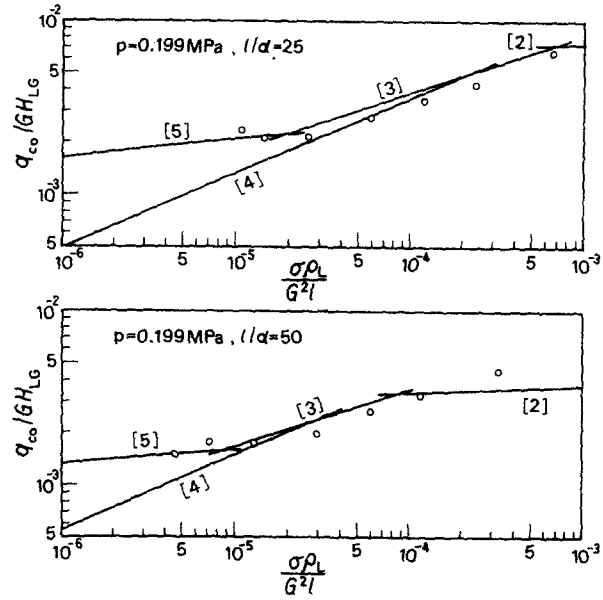

Figure 5. Comparison between the experimental and predicted q_{c0} for liquid helium ($l/d = 25$ and 50).

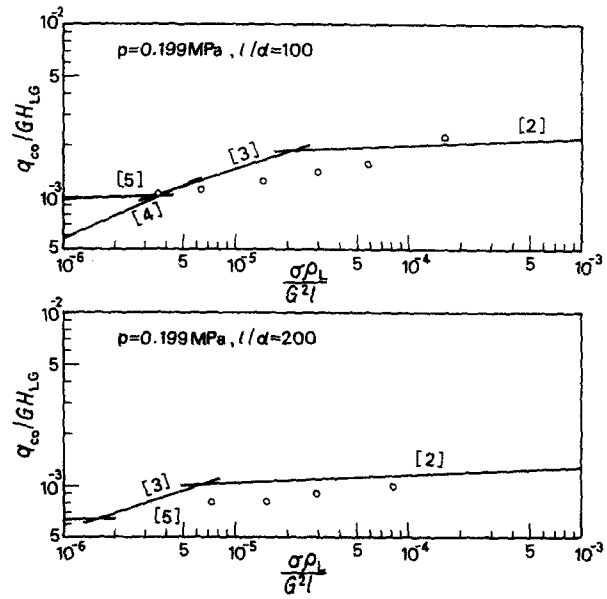

Figure 6. Comparison between the experimental and predicted q_{c0} for liquid helium ($l/d = 100$ and 200).

the heating over the section of 5 mm from the thermocouple to the exit end is neglected for simplicity's sake, then the upper diagram of figure 5 for example is replaced by figure 7. It seems likely, however, that there are no differences in trend between the above-mentioned two figures as far as the appearance of the high pressure character is concerned.

4.3 *Upper limit of mass velocity for detecting* CHF

There is the upper limit for the mass velocity capable of detecting CHF as has been described in section 3.2, which determines the lower limit of $\sigma\rho_L/G^2l$ of the data points

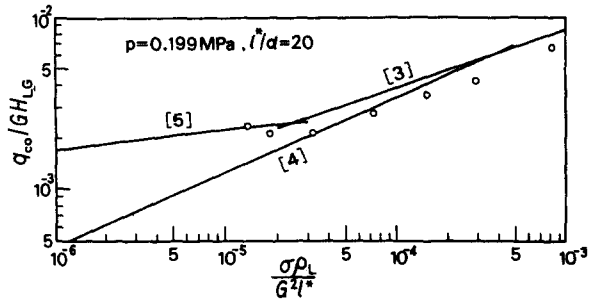

Figure 7. Effect of the location of the thermocouple to detect CHF.

in each diagram of figures 5 and 6. The cause to originate such low upper limits of the mass velocity has not yet been clear. However, it is certain that this phenomenon is not caused by the experimental apparatus employed in the present study. As an example of testing the apparatus with liquids other than liquid helium, a few CHF data of liquid nitrogen for $l/d = 200$ obtained with the same experimental apparatus are represented in figure 8, and the experimental q_{c0} obtained from these data is compared with the predicted q_{c0} in figure 9. As is seen in figure 8, liquid nitrogen at 0.220 MPa keeps on exhibiting the regular CHF even at the high magnitude of $G = 328$ kg m^{-2} s^{-1} as compared with the low limit value of $G = 52.6$ kg m^{-2} s^{-1} in the lower diagram of figure 4 for liquid helium.

It must be noted that the upper limit of G observed for the CHF of liquid helium is not connected with the so-called upstream CHF. About 20 years ago, Waters *et al.* (1964) carried out an experimental study on the CHF of water at $\rho_G/\rho_L = 0.0853$ for very high mass velocities $G = 6690$–9320 kg m^{-2} s^{-1}, observing the occurrence of the upstream CHF

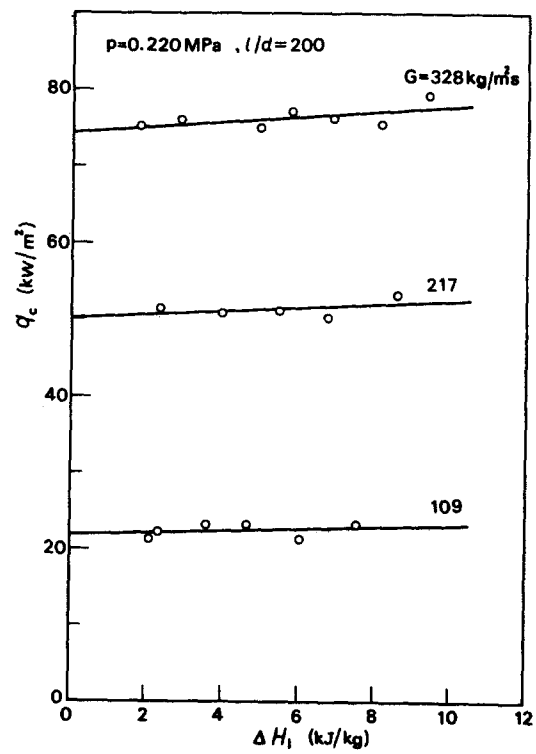

Figure 8. Experimental data of CHF of liquid nitrogen ($l/d = 200$).

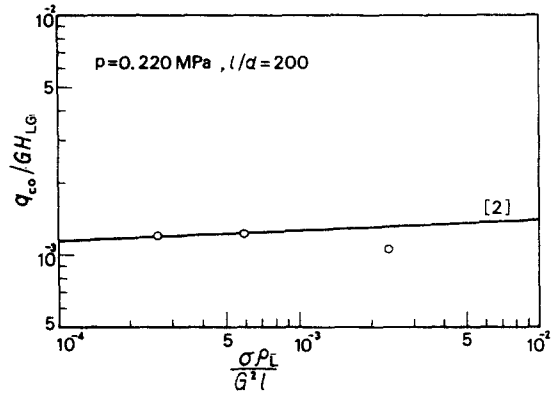

Figure 9. Comparison between the experimental and predicted q_{c0} for liquid nitrogen ($l/d = 200$).

in a range of ΔH_i near zero. Later, Collier (1972) referred to this phenomenon as the anomalous effects due to ultra-high mass velocities. Katto & Yokoya (1982) and Katto & Ashida (1982) reported that the same phenomenon as above takes place also in the case of R-12 at $\rho_G/\rho_L = 0.109$–0.306 when the mass velocity G is extremely high (say, $G > 3000\ \mathrm{kg\,m^{-2}\,s^{-1}}$). This upstream CHF is really an anomalous one that is specified with a very weak and slow temperature rise occurring at a position upstream of the tube exit end, so it bears some resemblance to the upper limit of G in respect of the weakening of the CHF phenonenon. However, the data points designated by solid circles in figures 3 and 4 are not those measured as the upstream CHF; that is, no CHF condition has been detected in this study by the thermocouples located sufficiently upstream of the exit end of the heated tube.

5. CONCLUSIONS

(1) The "basic critical heat flux" q_{c0} determined experimentally in this study for liquid helium at 0.199 MPa are found to be close to the prediction of [2] to [5] though somewhat regular deviations are observed when l/d is large.

(2) The high pressure character is found to appear in the CHF of liquid helium too, including the range of $l/d \leqq 51$, where no previous existing data have shown the high pressure character. However, the appearance of the high pressure character is restricted within a very narrow range of $\sigma\rho_L/G^2 l$ due to the existence of the upper limit of the mass velocity capable of detecting CHF.

Acknowledgements—We wish to acknowledge the financial support given by the Ministry of Education, Science and Culture to this study (Grant-in-Aid for Co-operative Research A: No. 0052033, 1980–82), and also, Messrs. N. Hieda and M. Watanabe for their assistance with the troublesome experiments.

REFERENCES

BECKER, K. M., DJURSING, D., LINDBERG, K., EKLIND, O. & ÖSTERDAHL, C. 1972 Burnout conditions for round tubes at elevated pressures. *Progress in Heat and Mass Transfer*, Vol. 6, pp. 55–74. Pergamon, Oxford.

CAMPOLUNGHI, F., CUMO, M., FERRARI, G., LEO, R. & VACCARO, G. 1974 Burn-out power in once-through tubular steam generators. *Proc. 5th Int. Heat Transfer Conf.*, Vol. IV, pp. 280–284.

CHOJNOWSKI, B. & WILSON, P. W. 1974 Critical heat flux for large diameter steam generating tubes with circumferential variable and uniform heating. *Proc. 5th Int. Heat Transfer Conf.*, Vol IV, pp. 260–264.

COLLIER, J. R. 1972 *Convective Boiling and Condensation,* 1st Edn, p. 259. McGraw-Hill, New York.

DOROSCHUK, V. E., LEVITAN, L. L. & LANTZMAN, F. P. 1975 Investigation into burnout in uniformly heated tubes. *ASME-Paper No. 75-WA/HT-22.*

GIARRATANO, P. J., HESS, R. C. & JONES, M. C. 1974 Forced convection heat transfer to subcritical helium I. *Advan. Cryogenic Engng* **19**, 404–416.

KATTO, Y. 1980a General features of CHF of forced convection boiling in uniformly heated vertical tubes with zero inlet subcooling. *Int. J. Heat Mass Transfer* **23**, 493–504.

KATTO, Y. 1980b Critical heat flux of forced convection boiling in uniformly heated vertical tubes (correlation of CHF in HP-regime and determination of CHF-regime map). *Int. J. Heat Mass Transfer* **23**, 1573–1580.

KATTO, Y. 1982 An analytical investigation on CHF of flow boiling in uniformly heated vertical tubes with special reference to governing dimensionless groups. *Int. J. Heat Mass Transfer* **25**, 1353–1361.

KATTO, Y. & ASHIDA, S. 1982 CHF in high-pressure regime for forced convection boiling in uniformly heated vertical tubes of low length-to-diameter ratio. *Proc. 7th Int. Heat Transfer Conf.*, Vol. 4, pp. 291–296.

KATTO, Y. & YOKOYA, S. 1982 CHF of forced convection boiling in uniformly heated vertical tubes: experimental study of HP-regime by the use of Refrigerant 12. *Int. J. Multiphase Flow* **8**, 165–181.

KEILIN, V. E., KOVALEV, I. A., LIKOV, V. V. & POZONKOV, M. M. 1975 Forced convection heat transfer to liquid helium I in the nucleate boiling region. *Cryogenics* **15**, 141–145.

LEE, D. H. 1970 Studies of heat transfer and pressure drop relevant to sub-critical once-through evaporators. *IAEA-SM-130156.* Int. Atomic Energy Agency, Vienna.

NISHIKAWA, K., YOSHIDA, S., YAMADA, A. & OHNO, M. 1982 Experimental investigation of critical heat flux in forced convection boiling of Freon in a tube at high subcritical pressure. *Proc. 7th Int. Heat Transfer Conf.*, Vol. 4, pp. 321–326.

OGATA, H. & SATO, S. 1973 Critical heat flux for two-phase flow of helium I. *Cryogenics* **13**, 610–611.

PESKOV, O. L., SUBBOTIN, V. I., ZENKEVICH, B. A. & SERGEYEV, N. D. 1969 The critical heat flux for the flow of steam–water mixtures through pipes. *Problems of Heat Transfer and Hydraulics of Two-Phase Media* (Edited by S. S. KUTATELADZE), pp. 48–62. Pergamon Press, Oxford.

THOMPSON, B. & MACBETH, R. V. 1964 Boiling water heat transfer burnout in uniformly heated tubes: a compilation of world data with accurate correlations. *UKAEA, AEEW-R* 356.

WATERS, E. D., ANDERSON, J. K., THRONE, W. L. & BATCH, J. M. 1964 Experimental observations of upstream boiling burnout. *Chem. Engng Prog. Symp. Ser.* **61**(57), 230–237.

WATSON, G. B. & LEE, R. A. 1974 Critical heat flux in inclined and vertical smooth and ribbed tubes. *Proc. 5th Int. Heat Transfer Conf.*, Vol. IV, pp. 275–279.